Enhancement of a multi-sided Bézier surface representation

Tamás Várady, Péter Salvi, István Kovács

Budapest University of Technology and Economics

Abstract

A new multi-sided surfacing scheme – the Generalized Bézier (GB) patch – has been introduced recently by Várady et al. [11]. The patch is created over a polygonal domain, its parameterization is defined by means of generalized barycentric coordinates. It has a simple control structure; the control points are associated with a combination of bi-parametric Bernstein functions, multiplied by rational terms. GB patches are compatible with adjacent quadrilateral Bézier patches and inherit most of their properties.

In this paper we present an enhanced version of the former scheme. The control structure has been slightly modified, yielding a perfect generalization of quadrilateral patches. The parameterization has also been altered, matching a concept of how quadrilateral domains transform to n-sided polygons. We propose improved blending functions and investigate how the weight deficiency of the basis functions can be distributed amongst control points. The former rational weighting functions have been modified to support not only G^1, but higher degree continuity between adjacent patches. After briefly discussing how degree reduction and elevation proceed, we present algorithms to automatically create and optimize the internal control points of GB patches. A few simple examples and suggestions for future work conclude the paper.

Keywords: general topology surfaces; multi-sided Bézier patches; barycentric parameterization; surface fitting

1. Introduction

The representation of multi-sided surface patches is an important issue when complex free-form objects need to be defined. There is a wide variety of choices, and contradictory requirements need to be prioritized to select the "best" for a given application. A general topology patchwork can be represented by trimmed tensor-product surfaces, but difficulties arise when boundaries need to be accurately interpolated or smooth connections need to be ensured. Recursive subdivision is another option, but forcing the limit surface to interpolate boundary curves with cross-derivatives is a hard problem. Multi-sided transfinite surfaces ensure watertight and smooth connections, and define the surface interior automatically, but this may be a disadvantage when the interior needs to be edited and optimized. Control point based multi-sided patches attempt to combine the merits of the previous representations, facilitating boundary interpolation and interior shape control.

The Generalized Bézier or GB patch is a recently published multi-sided patch formulation by Várady et al. [11]. It is fully compatible with tensor product Bézier patches and can interpolate arbitrary boundary curves and cross-derivatives given in Bézier form. The scheme produces a naturally distributed set of control points in the interior of the patch, that can be used for editing and optimization. In this paper we enhance the former representation. A modified control structure is proposed that is now in full accordance with that of quadrilateral patches. The new parameterization produces a better mapping. The modified blending functions resolve potential problems with the weight deficiency of the patch (see details later) and ensure high-degree continuous connections, as well.

In our view there are three main application areas where these patches can be utilized: (i) Aesthetic design of complex free-form objects is still a challenging task, and GB patches are very well suited for smoothly interpolating complex, general topology curve networks. (ii) Automatic hole filling in CAD systems is also an important problem, in particular where complex vertex blends are created. (iii) The approximation of 3D point clouds by a patchwork of smoothly connected multi-sided surfaces is also an interesting application.

The paper is structured in the following way. Related work is reviewed in Section 2. We reformulate the equations of quadrilateral Bézier patches and review the original multi-sided patch formulation, then introduce the modified

components in Section 3. Details of the modified parameterization and the new blending functions are presented in Section 4. Algorithms to determine the control points of GB patches, including degree reduction and elevation, merging interpolants of various degrees and applying least-squares approximation techniques are described in Section 5. Finally, a few examples are given to demonstrate useful features of GB patches in Section 6.

2. Previous work

General topology surfacing with multi-sided patchworks has a rich literature. In this section we refer to the most influential papers that describe multi-sided generalizations of Bézier patches.

1. There is a line of research where patches are parameterized by n variables connected by a system of constraints. Three- and five-sided patches with quadratic boundaries were defined in the early work of Sabin [8]; a similar method with cubic boundaries was proposed by Hosaka and Kimura [3]. These patches were generalized by Zheng and Ball [14] for arbitrary degree d, with a control structure that is almost identical to ours. It is important to note that the solution of the implicit constraint system is known only for $n \leq 6$. There is no direct mapping from a domain; two independent variables are chosen instead, and the other variables are determined by the constraints. This may lead to difficulties when geometric computations (e.g. intersections) need to be performed on these patches. Exact degree elevation can be achieved through a fairly complex algebra, see Ball and Zheng [1]. On cyclic parameterizations, see also the interesting conjecture by Sabin [9].
2. The S-patch of Loop and DeRose [6] represent another generalization of quadrilateral (and triangular) Bézier surfaces, with many nice mathematical properties. General barycentric coordinates are computed for the points of an n-sided polygonal domain, and multi-variate Bernstein functions are applied to them. Each term contains a product of n barycentric coordinates, where their exponents sum up to the degree of the patch. For many sides and/or a high degree the number of possible permutations increase fast, and this yields a lot of control points in a peculiar arrangement, hardly suitable for interactive design. At the same time, the approach inherits all the favorable properties of Bézier patches: the degree elevation algorithm and the creation of patches within another patch emerge naturally from the theory.
3. Multi-sided patches can also be created by "cutting off" parts of a Bézier triangle with the help of base points, see Warren [13]. Due to the construction, there is an inherent asymmetry between the sides of the patch. This method only allows $n \leq 6$, as well. A generalization of this idea is the toric patch by Krasauskas [5]. This surface is defined over a polygon on an integer lattice – an interesting, but slightly limited construction. G^1 continuity between surfaces is complex, but possible, see Sun and Zhu [10].

In this paper we will focus on a new representation – the GB patches – published recently by Várady et al. [11]. It is defined over a regular polygonal domain, and has a simple and symmetric control structure. The patch is described by $2n$ local parameters, derived from general barycentric coordinates. Combinations of rationally weighted bivariate Bernstein blending functions are used, allowing various number of sides ($n \geq 3$) and degrees ($d \geq 3$). As our current work is a modification of the former GB patch, we will give a more thorough review in Section 3, and then present various improvements concerning the control structure, the parameterization and the blending functions.

3. Generalized Bézier patches

First let us revisit four-sided Bézier patches and reformulate the related surface equations, as this will help introducing the multi-sided GB patches. The key idea is that the same control points can be associated with two adjacent sides and multiplied by two families of blending functions. It will be proven that GB patches behave as ordinary four-sided Bézier patches along their boundaries, and at the same time provide natural, smooth transitions in the interior.

3.1. Quadrilateral Bézier patches

A degree d quadrilateral Bézier patch is defined over a rectangular domain $0 \leq u, v \leq 1$ as

$$S(u,v) = \sum_{j=0}^{d} \sum_{k=0}^{d} C_{j,k}^{d} B_{j,k}^{d}(u,v). \tag{1}$$

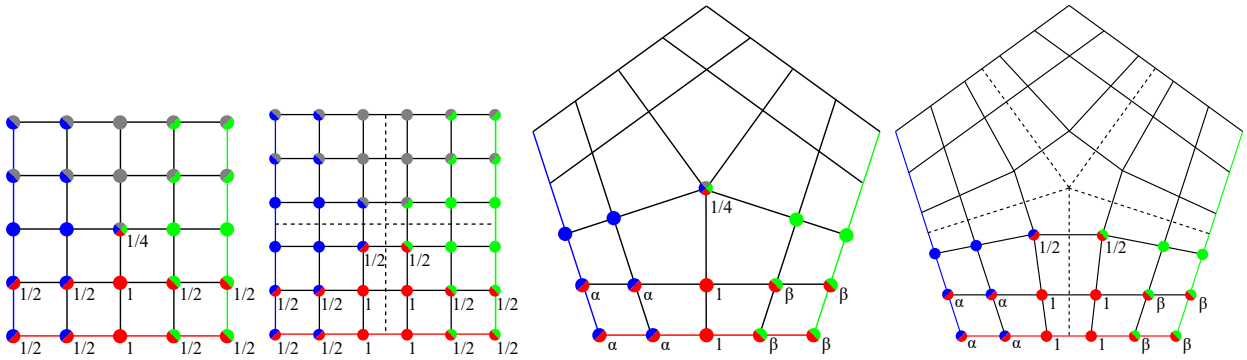

(a) $n = 4, d = 4$ (b) $n = 4, d = 5$ (c) $n = 5, d = 4$ (d) $n = 5, d = 5$

Figure 1: Control points associated with the sides of the domain for quadrilateral and n-sided patches. Values of the weighting functions $\mu^i_{j,k}$ are shown for the bottom (red) ribbon.

The control points $C^d_{j,k}$ form a regular grid and are multiplied by bi-parametric Bernstein polynomials $B^d_{j,k}(u,v) = B^d_j(u) \cdot B^d_k(v)$. Let us rearrange this equation by grouping the control points by sides, using circular indexing. Group i contains those control points that are closer to side i than to the other sides. For example, in Figure 1a the bottom two rows of a bi-quartic patch (in red) belong to side 1, the two columns on the right (in green) to side 2, and so on. For a bi-quintic patch in Figure 1b the bottom three rows of control points are associated with side 1, and the three columns on the right with side 2, etc. We refer to these groups of control points as *ribbons,* each of which consists of $l = \lfloor (d+1)/2 \rfloor$ control point rows or *layers*, each layer containing $d+1$ control points. In the case of even-degree patches, the center control point is also taken into consideration, supplementing the four ribbons.

Let us introduce local *side* and *distance* parameters (s_i, h_i), that are associated with each side: s_i takes values between 0 and 1 as it sweeps from the "left" to the "right" side; while h_i is zero on the base side and increases monotonically to 1 as it approaches the opposite side. In the quadrilateral case this can be achieved simply by setting

$$\begin{aligned} s_1 &= u, & s_2 &= v, & s_3 &= 1-u, & s_4 &= 1-v, \\ h_1 &= v, & h_2 &= 1-u, & h_3 &= 1-v; & h_4 &= u. \end{aligned} \tag{2}$$

The Bernstein functions of h_i guarantee that the i-th ribbon will have no effect on the opposite side, neither in positional, nor in differential sense. Thus a side-based equation can be rearranged as the sum of four ribbons and an additional center term, needed only when d is even:

$$S(u,v) = \sum_{i=1}^{4} \sum_{j=0}^{d} \sum_{k=0}^{l-1} C^{d,i}_{j,k} \mu^i_{j,k} B^d_{j,k}(s_i, h_i) + \begin{cases} C^d_{l,l} \sum_{i=1}^{4} \mu^i_{l,l} B^d_{l,l}(s_i, h_i) & \text{when } d \text{ is even,} \\ \mathbf{0} & \text{when } d \text{ is odd.} \end{cases} \tag{3}$$

Here the indexing scheme is side-based: $C^{d,i}_{j,k}$ refers to the j-th control point in the k-th row of the i-th side. The control points are multiplied by various scalar weights $\mu^i_{j,k}$. Some of these are assigned only to a single ribbon ($\mu^i_{j,k} = 1$), others – around the corners of the patch – occur in two adjacent ribbons and are weighted by $\mu = \frac{1}{2}$. For example, take the bi-quartic patch, then $C^{4,1}_{3,1}$ and $C^{4,2}_{1,1}$ refer to the same control point. The center control point of even-degree patches is shared by four ribbons and is weighted by $\mu = \frac{1}{4}$. The weights associated with each control point always sum up to 1. This also implies that control points with $\mu^i_{j,k} = 1$ will obtain weights $\mu^{i-1}_{d-k,j} = 0$ or $\mu^{i+1}_{k,d-j} = 0$ from the adjacent ribbons. The colored structure of the control points and the related weights for the bottom side are depicted in Figures 1a–1b. Below we also give a formal definition of the $\mu^i_{j,k}$-s on the left side (i.e., when $j \le d/2$), the right side can be derived in a symmetric manner:

$$\mu^i_{j,k} = \begin{cases} 0 & j < k \text{ and } k \ge 2, \\ \frac{1}{2} & j = k < l \text{ or } j + k < 2, \\ 1 & \text{otherwise,} \end{cases} \tag{4}$$

and $\mu^i_{l,l} = \frac{1}{4}$ for the common center point.

For quadrilateral Bézier patches the sum of the weighting functions equals to 1 everywhere in the domain, i.e.,

$$B^d_{\mathrm{All}}(u,v) = \sum_{i=1}^{4}\sum_{j=0}^{d}\sum_{k=0}^{l-1}\mu^i_{j,k}B^d_{j,k}(s_i,h_i) + \begin{cases}\sum_{i=1}^{4}\mu^i_{l,l}B^d_{l,l}(s_i,h_i) & \text{when } d \text{ is even}\\ 0 & \text{when } d \text{ is odd}\end{cases} = 1. \tag{5}$$

3.2. The former Generalized Bézier patch

The decomposition of the rectangular control grid into side-based ribbons led to the formulation of the former n-sided GB patch, see Várady et al. [11]. Here the local parameters (s_i, h_i) of each side were defined over a regular n-sided polygon with similar properties as before: h_i vanishes on the base side and equals to 1 on *all* the "opposite" sides. While their relationship is fairly simple in the four-sided case, more complex constructions are needed for polygons. Related parameterizations using general barycentric coordinates will be discussed in Section 4.1.

In the multi-sided case the weighted bi-parametric Bernstein functions do not naturally add up to 1, which is needed for affine invariance. In the former GB patch scheme this is resolved by assigning a special blending function B^d_0 to the central control point C^d_0, that accumulates all the weight deficiency. Note that this control point exists for patches of odd degree, as well. The surface equation becomes

$$S(u,v) = \sum_{i=1}^{n}\sum_{j=0}^{d}\sum_{k=0}^{l-1}C^{d,i}_{j,k}\mu^i_{j,k}B^d_{j,k}(s_i,h_i) + C^d_0B^d_0(u,v). \tag{6}$$

In this construction the weights $\mu^i_{j,k}$ gain a different meaning. The tricky issue here is how to combine two-variate parameterizations to maintain G^1 (or G^2) continuity on the patch boundaries. Some of the $\mu^i_{j,k}$ values will become *functions* of adjacent distance parameters, such as $\mu^i_{j,k}(h_{i-1}, h_i)$ or $\mu^i_{j,k}(h_i, h_{i+1})$, instead of constants. Related issues concerning various weights, blending functions and continuity will be discussed in Section 4.2.

Experiments with the first GB patch were very positive, however, forthcoming analysis brought up interesting issues. One observation was that the weight deficiency significantly increases when the number of sides and/or the degree is large. This means that the influence of the central control point becomes relatively strong as n and d grow. We have also noticed that the weight deficiency strongly oscillates between the even and odd degrees when increasing the degree of the patch, in contrast to the expected monotonity.

3.3. The new GB patch representation

The goal of this paper is to introduce a new GB patch, that resolves the above mentioned problems and yields a better matching generalization of the quadrilateral scheme of Section 3.1. For odd-degree patches we do *not* use a central control point; for even-degree patches we bring back the center point with its original meaning and assign a well-defined weight to it as the sum of weights of the quadrilateral central points associated with the ribbons, see Eq. (3). Accordingly a new surface equation is obtained:

$$S(u,v) = \sum_{i=1}^{n}\sum_{j=0}^{d}\sum_{k=0}^{l-1}C^{d,i}_{j,k}\mu^i_{j,k}\hat{B}^d_{j,k}(s_i,h_i) + \begin{cases}C^d_{l,l}\sum_{i=1}^{n}\mu^i_{l,l}B^d_{l,l}(s_i,h_i) & \text{when } d \text{ is even,}\\ \mathbf{0} & \text{when } d \text{ is odd.}\end{cases} \tag{7}$$

Here we distribute the weight deficiency among the blending functions of the innermost ring, resulting in new blending functions $\hat{B}^d_{j,k}$:

$$\hat{B}^d_{j,k}(s_i,h_i) = B^d_{j,k}(s_i,h_i) + \begin{cases}\left(1 - B^d_{\mathrm{All}}(u,v)\right)/N & \text{when } k = l-1,\\ 0 & \text{otherwise,}\end{cases} \tag{8}$$

where the total blend is computed as

$$B^d_{\mathrm{All}}(u,v) = \sum_{i=1}^{n}\sum_{j=0}^{d}\sum_{k=0}^{l-1}\mu^i_{j,k}B^d_{j,k}(s_i,h_i) + \begin{cases}\sum_{i=1}^{n}\mu^i_{l,l}B^d_{l,l}(s_i,h_i) & \text{when } d \text{ is even}\\ 0 & \text{when } d \text{ is odd.}\end{cases} \tag{9}$$

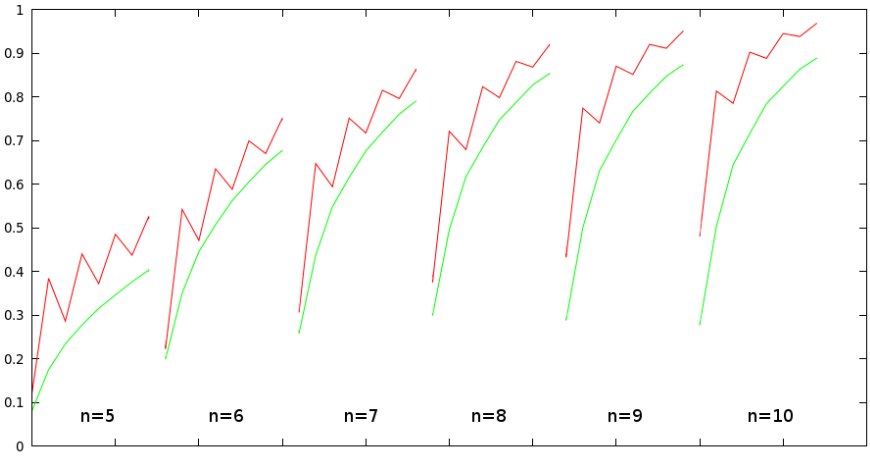

Figure 2: Comparing weight deficiencies between the former (red) and the new (green) constructions. Each series shows the values for $d = 3 \dots 10$.

While in principle it is possible to modify the original blending functions for an arbitrary set of control points, in Eq. (8) we chose to apply this only for the innermost ring, that involves $N = n$ control points for odd-degree patches, and $N = 2n$ for even-degree patches. (Note, that each control point in the innermost ring gets an $1/N$-th part of the weight deficiency, since the scaling function μ always adds up to 1, i.e., $\mu^i_{j,k} + \mu^{i-1}_{d-k,j} = 1$ or $\mu^i_{j,k} + \mu^{i+1}_{k,d-j} = 1$.) For $n = 3$ the weight deficiency is negative, and in this case we retain the original patch formulation.

The new approach produced more natural, monotone weight deficiencies with respect to the degrees. The difference is demonstrated in Figure 2. The overweight of the central control point has also been reduced. Two new GB patches – a quartic and a quintic – are shown in Figure 3.

4. Components of the GB scheme

In this section we describe further details of the GB construction, including parameterization, blending functions, and smooth (G^1/G^2) connection to adjacent patches.

4.1. New Parameterization

Parameterization by the local parameters (s_i, h_i) determines the mapping from the domain to 3D, and thus influences the shape of the surface. For GB patches we have chosen parameterizations that are based on generalized barycentric coordinates $\lambda_i = \lambda_i(u, v)$, $i = 1 \dots n$. There are several publications that thoroughly analyze their properties, see for example Floater [2]. It is well-known that $\lambda_i \geq 0$ (positivity) and $\sum \lambda_i = 1$ (partition of unity) hold for

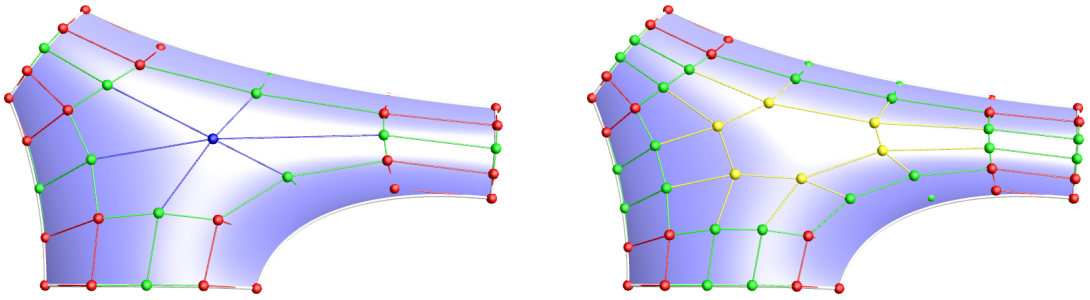

(a) $n = 6, d = 4$ (b) $n = 6, d = 5$

Figure 3: Examples of the new Generalized Bézier patch.

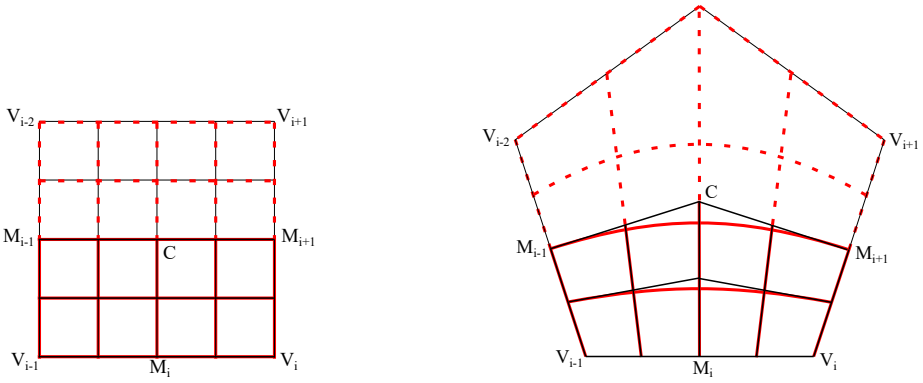

(a) Four-sided patch (b) Five-sided patch

Figure 4: Transition from quadrilateral to multi-sided patches.

all points within a convex domain. For the vertices of the polygon $\lambda_i = \delta_{ij}$ (Lagrange property) is satisfied, where δ_{ij} is the Kronecker delta. While the generalized barycentric coordinates are associated with the vertices of the polygon, the s_i and h_i parameters are related to the individual sides. We exploit the above properties and create a bivariate parameterization for each ribbon over the full polygon. In the former GB patch the authors have proposed the following mapping (see also Figure 5a):

$$s_i(u,v) = \frac{\lambda_i}{\lambda_{i-1} + \lambda_i}, \qquad h_i(u,v) = 1 - \lambda_{i-1} - \lambda_i. \tag{10}$$

The side parameter s_i varies from 0 to 1 on side i, with $s_i = 0$ on side $i-1$, and $s_i = 1$ on side $i+1$. For all other points, s_i takes values between 0 and 1. The distance parameter h_i vanishes on side i, since this is the only place where the sum $\lambda_{i-1} + \lambda_i$ equals to 1. It increases linearly from 0 to 1 on sides $i-1$ and $i+1$. On all remaining ("distant") sides h_i equals to 1 (cf. the quadrilateral case, where it is 1 only on the opposite side). On side i the equations $s_i = h_{i-1}$ and $s_i = 1 - h_{i+1}$ are also satisfied. We prefer using Wachspress coordinates, since they produce straight lines for the s_i constant parameter curves.

This parameterization works nicely, however, we have decided to improve the h_i isolines, providing a better isoline distribution in the interior of the polygon. This also affects the 3D mapping of the isolines on the surface and favorably relocates the footpoints of the blending functions.

We define the fullness of the h_i isolines by an intuitive method, that describes how a four-sided domain transforms into a polygonal one. Take the quadrilateral in Figure 4a with base side $\overline{V_{i-1}V_i}$, and imagine the edges $i-1$ and $i+1$ starting to rotate outwards to form an n-sided polygon. Midpoints M_{i-1} and M_{i+1} move away from each other, center C moves upwards, and eventually the original small rectangle $\overline{M_{i-1}V_{i-1}M_iC}$ transforms into a rhombus, see Figure 4b. We assume that the middle isoline h_i that connects M_{i-1} and M_{i+1} remains perpendicular to sides $i-1$ and $i+1$ during the process. Accordingly, it is a natural choice for the new GB patch to define a parametrization where the $h_i = \frac{1}{2}$ constant parameter line approximates an imaginary circular arc, i.e., it is tangential to the chords $\overline{M_{i-1}C}$ and $\overline{M_{i+1}C}$, and its middle point P is constrained to the middle point of the circular arc. The former parameterization has been extended by two correction terms:

$$h_i(u,v) = 1 - \lambda_{i-1} - \lambda_i - W_i^1(\lambda_1, \ldots, \lambda_n) + W_i^2(\lambda_1, \ldots, \lambda_n), \tag{11}$$

where W_i^1 is to set the tangential criteria, and W_i^2 the midpoint constraint, see details in Appendix A.

The former and the new parameterizations can be compared in Figure 5. Observe that the h_i parameter lines are *almost* tangential to the corresponding s_{i-1} and s_{i+1} parameter lines, although we have constrained tangency only at $h_i = \frac{1}{2}$.

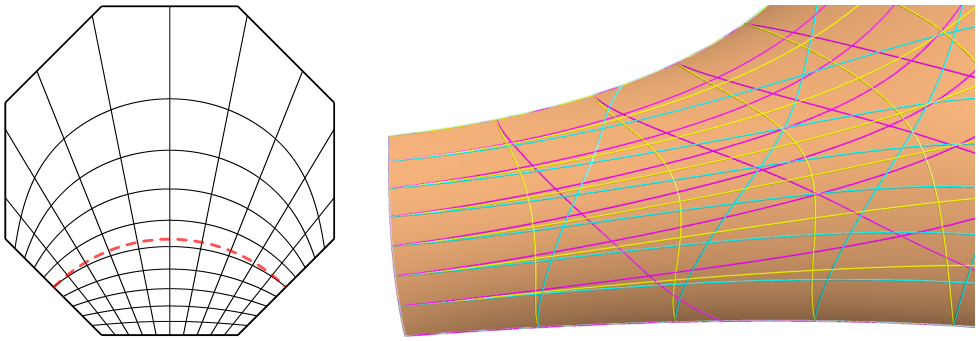

(a) Former parameterization

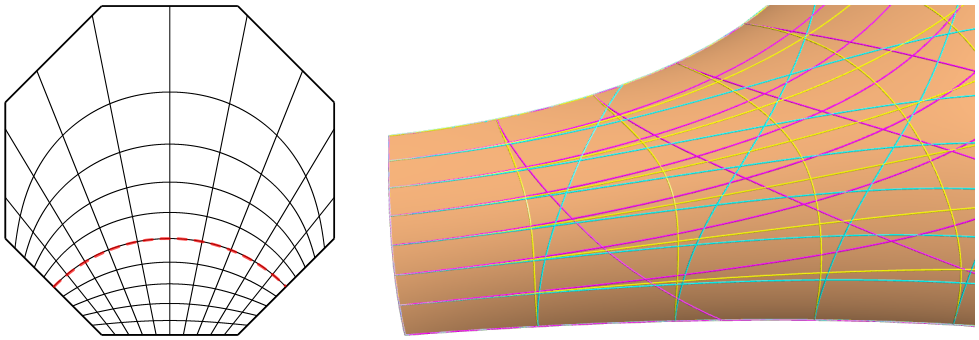

(b) New parameterization

Figure 5: Comparison of constant parameter lines in the domain and in 3D.

4.2. Blending functions and continuity

As we have seen in Section 3, the blending functions associated with the control points are multiplied by weighting functions $\mu^i_{j,k}$. These are constant weights defined similarly to the quadrilateral case, except at 2×2 control points near the corners, where they are computed by functions $\alpha_i = \alpha_i(h_i, h_{i-1})$ and $\beta_i = \beta_i(h_i, h_{i+1})$, see Figures 1c–1d. Formally we define $\mu^i_{j,k}$ for the left side (i.e., $j \le d/2$) as follows:

$$\mu^i_{j,k} = \begin{cases} 0 & j < k \text{ and } k \ge 2, \\ \frac{1}{2} & 2 \le j = k < l, \\ \alpha_i & j, k < 2, \\ 1 & \text{otherwise}, \end{cases} \tag{12}$$

and $\mu^i_{l,l} = \frac{1}{4}$ for the common center point (when exists). The equation for the right side is analogous, using β_i instead of α_i. In the former GB patch α_i and β_i were defined as

$$\alpha_i = \frac{h_{i-1}}{h_{i-1} + h_i}, \qquad \beta_i = \frac{h_{i+1}}{h_{i+1} + h_i}. \tag{13}$$

Note that $\alpha_i = 0$ for points on side $i-1$, $\beta_i = 0$ for points on side $i+1$, and $\alpha_i = \beta_i = 1$ on side i (with singularities at the corners). These rational functions determine which blending function ($B^i_{j,k}$ vs. $B^{i-1}_{d-k,j}$ or $B^{i+1}_{k,d-j}$) is dominant in the vicinity of the corresponding sides.

Let us define a G^1 *side interpolant* $I_i(s_i, h_i)$ as a classical Bézier patch of degree $d \times 1$, created by the first two layers of control points for each side:

$$I_i(s_i, h_i) = \sum_{j=0}^{d} \sum_{k=0}^{1} C^{d,i}_{j,k} B^d_{j,k}(s_i, h_i). \tag{14}$$

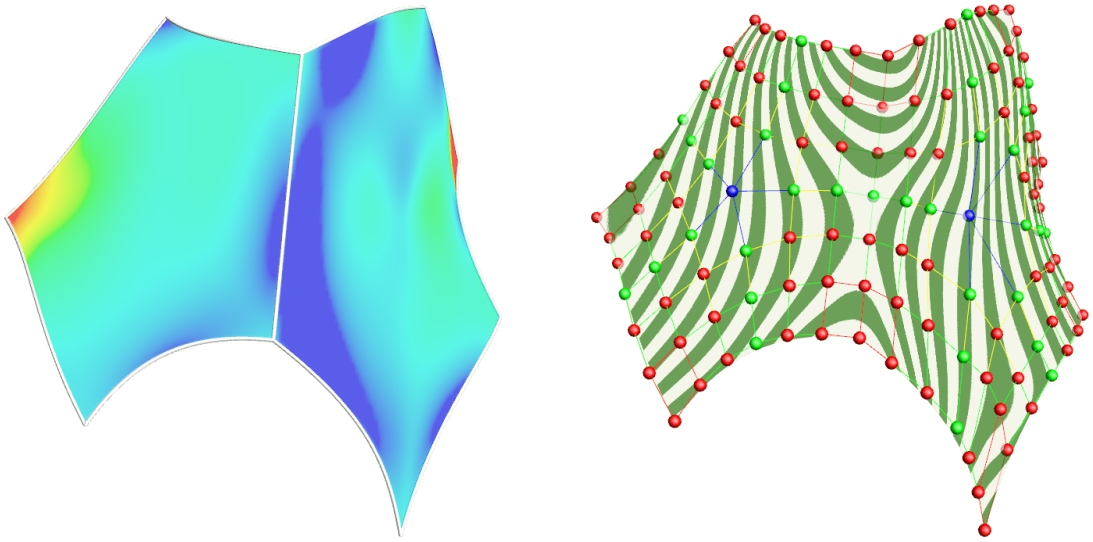

(a) Mean curvature and boundary curves

(b) Isophote lines and control points

Figure 6: Connecting GB patches with curvature continuity.

It was proven that using the above α_i and β_i functions, the Generalized Bézier patch interpolates the boundary and the first cross-derivatives of the G^1 side interpolants on its respective sides, i.e., $S(u,v) = I_i(s_i, 0)$ and $S'(u,v) = I_i'(s_i, 0)$ hold for all (u,v) points on the i-th side, see Várady et al. [11]. (In this context, we use the notation f' for directional derivatives in an arbitrary direction in the domain.) This condition is sufficient to get connected to other quadrilateral or multi-sided patches with G^1 continuity. If the adjacent side interpolants are G^1-compatible, then the n-sided patches will also be connected with tangential continuity, independently of their interior.

In the new GB patch we propose a slightly modified equation for α_i and β_i:

$$\alpha_i = \frac{h_{i-1}^2}{h_{i-1}^2 + h_i^2}, \qquad \beta_i = \frac{h_{i+1}^2}{h_{i+1}^2 + h_i^2}. \tag{15}$$

By using squared distance parameters, the proof of G^1 interpolation becomes simpler, and G^2 connections can also be ensured. It is important to notice that the i-th side of the GB patch is affected only by ribbons $i-1$, i and $i+1$, since the distance parameters h_j of the other sides will be 1 there, thus the related Bernstein functions and their first derivatives vanish, as all of them contain terms $(1-h_j)^{d-k}$, $k < d/2$. Another observation is that the control points $C_{j,k}^{d,i-1}$ $(j \le d-2)$ and $C_{j,k}^{d,i+1}$ $(j \ge 2)$ do not affect the i-th side due to the related Bernstein functions with $s_{i-1} = 1$ and $s_{i+1} = 0$. Therefore the effect of the adjacent sides depends only on the blending functions associated with the $2x2$ control points at the corners (colored red in Figure 3). We also have $\beta_{i-1} = \alpha_{i+1} = 0$ and $\beta_{i-1}' = \alpha_{i+1}' = 0$, so there neither will be any positional or derivative contribution from side $i-1$ and $i+1$. At the same time, $\alpha_i = \beta_i = 1$, so all control points of the G^1 side interpolant (i.e., the first two rows) appear with $\mu_{j,k}^i = 1$ weight in the patch equation.

For G^2 interpolation we assume that the GB patch has at least three layers, and accordingly the G^2 side interpolant is a Bézier patch of $d\times 2$ degrees. Analogously to the G^1 case, here we need to deal only with the 3×3 control points in the corners, each multiplied with the related α and β terms. The second derivatives of these functions at a point on side i is

$$\alpha_{i+1}'' = 2(h_i')^2/h_{i+1}^2, \qquad \beta_i'' = -2(h_i')^2/h_{i+1}^2, \tag{16}$$

so $\alpha_{i+1}'' + \beta_i'' = 0$. Without loss of generality, take a control point $C_{j,k}^i = C_{k,d-j}^{i+1}$ in the "right" corner where $\mu_{j,k}^i = \beta_i$. Its associated blending function is $\beta_i B_{j,k}^d(s_i, h_i) + \alpha_{i+1} B_{k,d-j}^d(s_{i+1}, h_{i+1})$. Also note, that these two Bernstein functions are equal, since $s_i = 1 - h_{i+1}$ and $h_i = s_{i+1} = 0$ at a point on side i. Then, using the property $\beta_i' = 0$, the second derivative

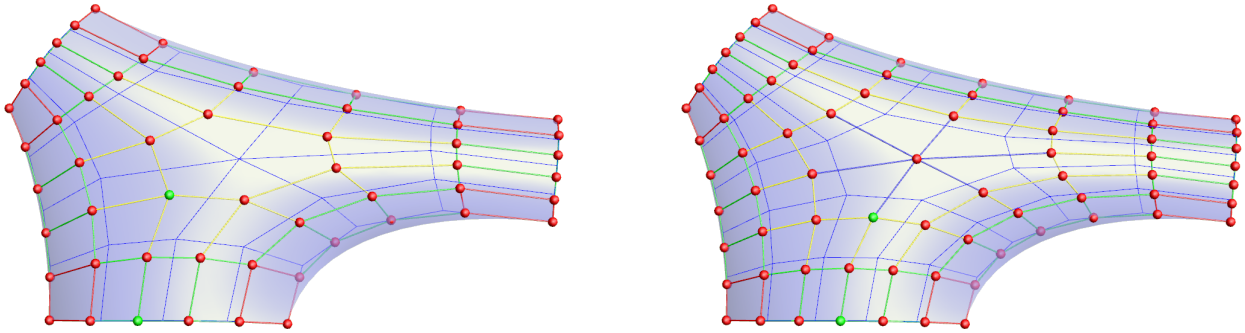

(a) Quartic to quintic

(b) Quintic to sextic

Figure 7: Degree elevation.

can be written as

$$\begin{aligned}\left(\beta_i B^d_{j,k}(s_i,h_i)+\alpha_{i+1}B^d_{k,d-j}(s_{i+1},h_{i+1})\right)'' &= \beta_i B''^d_{j,k}(s_i,h_i)+\beta_i'' B^d_{j,k}(s_i,h_i)+\alpha_{i+1}'' B^d_{k,d-j}(s_{i+1},h_{i+1})\\ &= 1\cdot B''^d_{j,k}(s_i,h_i)+(\alpha_{i+1}''+\beta_i'')\cdot B^d_{j,k}(s_i,h_i)\\ &= B''^d_{j,k}(s_i,h_i),\end{aligned} \tag{17}$$

and this is what we wanted to prove. Figure 6 shows a five-sided and a six-sided GB patch connected with G^2 continuity. The control points in the first three rows of these patches are set up in exactly the same way as it is done for four-sided Bézier patches, see e.g. Kahmann [4].

For completeness' sake, we still need to show that distributing the weight deficiency does not harm the interpolation property. This is a corollary of the above proof – we have shown, that the n-sided patch behaves like the G^1 or G^2 side interpolant at its boundary, with the same blending functions. But the side interpolant does not have weight deficiency, consequently it must be zero for the n-sided patch, as well.

5. Algorithms

In this section we present a few algorithms related to GB patches. First we summarize degree elevation and reduction (see also Várady et al. [11]), as this is necessary to understand the next subsections.

5.1. Degree elevation and reduction

Degree elevation proceeds according to the basic rules of Bézier curves and quadrilateral Bézier surfaces. For a degree d control polygon, new control point positions are computed on each boundary chord by the linear combination

$$C^{d+1,i}_{j,0}=\gamma_j C^{d,i}_{j-1,0}+(1-\gamma_j)C^{d,i}_{j,0}, \qquad \gamma_j=\frac{j}{d+1}, \quad 1\le j\le d. \tag{18}$$

Inside each quadrangle of the control structure a bilinear combination of the vertices is used:

$$C^{d+1,i}_{j,k}=\gamma_j\delta_k C^{d,i}_{j-1,k-1}+(1-\gamma_j)\delta_k C^{d,i}_{j,k-1}+\gamma_j(1-\delta_k)C^{d,i}_{j-1,k}+(1-\gamma_j)(1-\delta_k)C^{d,i}_{j,k}, \tag{19}$$

where $\gamma_j=\frac{j}{d+1}$, $\delta_k=\frac{k}{d+1}$, $1\le j\le d$ and $1\le k\le l$. (Note that the indexing scheme is naturally extended to interpret control points $C^{d,i}_{j,l}$ as $C^{d,i-1}_{d-l,j}$ or $C^{d,i+1}_{l,d-j}$.)

In Figure 7a a quartic to quintic degree elevation is shown. The blue lines show the initial quartic control net; the colored control points are the new ones inserted on the chords and in the quadrangles. When elevating from an even to an odd degree, the central control point also affects the odd-degree structure, see e.g. the green control point in the interior quadrangle. Figure 7b shows a quintic to sextic degree elevation; when going from an odd to an even degree, the central control point is inserted as the centroid of the control points in the innermost ring.

It must be emphasized that degree elevation does not produce an identical GB surface, as in the case of tensor product Bézier patches. The above procedure creates an elevated network, but the weights of the control points are computed by different blending functions and different weight deficiencies (see Section 4.2). The boundaries and cross-derivatives are preserved, but the interior of the elevated patch only approximates the original patch. The difference is minor, as it is illustrated in Section 6.1, where deviations between the original and the degree elevated patches are given. It is also shown there that by optimizing the interior control points of the degree $d+1$ patch, both the maximum and the average deviations can be drastically reduced.

Concerning degree reduction, our preference was to perform an "inverse" degree elevation. For the boundary curves, we proceed from the corners towards the middle of the degree $d+1$ control polygon by rearranging the above formulae. Using index j once from 1 upwards, then from d downwards, we obtain the following pairs of equations:

$$C^{d,i}_{j,0} = \frac{C^{d+1,i}_{j,0} - \gamma_j C^{d,i}_{j-1,0}}{1-\gamma_j}, \qquad 1 \le j \le m, \tag{20}$$

$$C^{d,i}_{j-1,0} = \frac{C^{d+1,i}_{j,0} - (1-\gamma_j) C^{d,i}_{j,0}}{\gamma_j}, \qquad d-m+1 \le j \le d, \tag{21}$$

where $m = \lfloor d/2 \rfloor$. This yields a unique solution when we move from even to odd degrees, however, it is ambiguous in the odd-to-even-degree case, where two different middle control points are obtained; these need to be averaged for the final structure. Degree reduction for the interior control points proceeds in a similar way, by moving from the corners inwards quadrangle by quadrangle; in each case we already have three control points of degree d and the fourth missing control point is determined from the internal $C^{d+1,i}_{j,k}$, e.g.:

$$C^{d,i}_{j,k} = \frac{C^{d+1,i}_{j,k} - \gamma_j \delta_k C^{d,i}_{j-1,k-1} - (1-\gamma_j)\delta_k C^{d,i}_{j,k-1} - \gamma_j(1-\delta_k) C^{d,i}_{j-1,k}}{(1-\gamma_k)(1-\delta_k)}. \tag{22}$$

Imagine now that in Figure 7 we calculate the degree d blue control net from the degree $d+1$ colored control points. For the odd-to-even case, averaging is needed at control points $C^{d,i}_{m,k}$. The central control point of even degree patches is computed as the average of the individual central control points extrapolated from each interior quadrangle.

5.2. Merging G^1 side interpolants of various degrees

The degree elevation and reduction mechanism in the previous section makes it possible to merge interpolants of different degrees into a single GB patch. First successive degree reductions are performed on all interpolants down to degree 3, and a GB patch with cubic boundaries and cross-derivatives is created. During this process control points of the side interpolants at each degree are saved for future use. Then repeated degree elevations are performed step-by-step. At an intermediate degree $\hat{d}$, the interior control points are first redefined by the rules of degree elevation, and then the external two rows of control points are restored from the saved values (when the interpolant was at least of degree $\hat{d}$). The process is continued until $\hat{d}$ reaches the highest degree of the interpolants. Therefore the interpolants get reproduced, and the missing interior control points get inserted in a natural manner as the degree is raised. This mechanism can be applied to merge G^2 interpolants as well, if the number of layers is at least 3 (in this case, the patch is reduced to degree 5 in the first step). An example is given in Section 6.2, see Figures 11c–11d.

5.3. Fullness control

The interpolant merging algorithm in the previous section yields default positions for the internal control points. This procedure also offers an opportunity to adjust the fullness of the surface by editing some control points at a lower-degree state. This is in parallel with the well-known subdivision modeling technique, where large-scale changes are accomplished by using a low-resolution mesh. The central control point of the quartic patch is particularly suited for this kind of control, as the designer can move the whole set of inner control points in a natural way, by modifying only this single control point. We have found that explicitly fixing the central control point position in addition to the side interpolants is a convenient way to adjust the fullness of the final patch.

In this case, merging the interpolants proceeds in a somewhat different manner. Assume that a central control point has been specified. The algorithm starts the same way, by creating a cubic patch. Then we perform successive

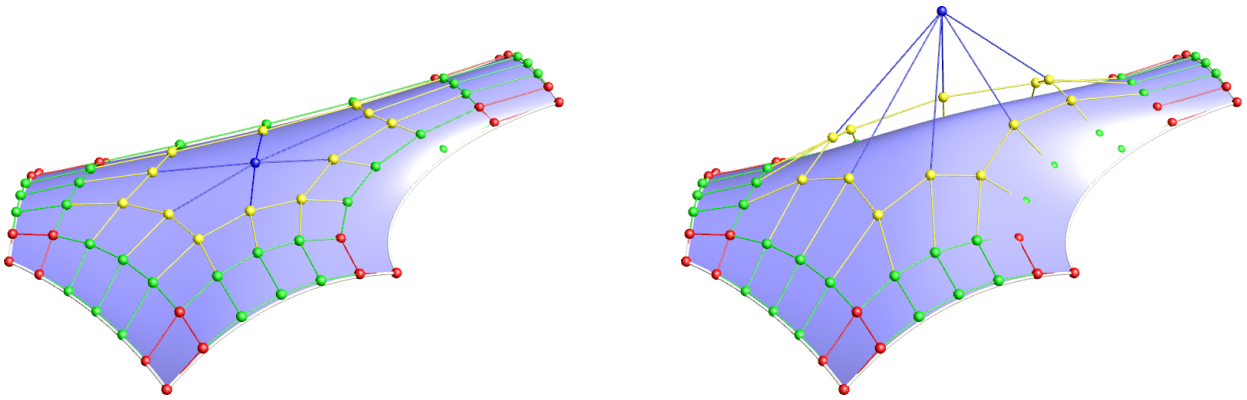

(a) Control points solely based on side interpolants

(b) Surface generated with a fixed central control point

Figure 8: Fullness control example.

degree elevations and correct the boundary control points, as before, but in even-degree patches we also fix the central control point position to the specified location instead of the centroid. Due to the elevation process, this has a global effect on the internal control points. The result of this process is illustrated in Figure 8, where the default patch and the one with fullness control can be compared.

5.4. Approximation of point clouds

Given an initial surface S with data points P_i and associated parameters (u_i, v_i), we wish to minimize the expression

$$\sum_i (S(u_i, v_i) - P_i)^2 = \min, \tag{23}$$

which leads to a linear system of equations in the unknown control points $C^{d,i}_{j,k}$ and $C^d_{l,l}$ (when d is even). Each control point except the central one appears with two indices in Equation (7), but we can avoid the ambiguity with the constraint $j \leq \lfloor d/2 \rfloor$. Now the blending function associated with $C^{d,i}_{j,k}$ is

$$\mu^i_{d-k,j} \hat{B}^d_{d-k,j}(s_i, h_i) + \mu^{i+1}_{j,k} \hat{B}^d_{j,k}(s_{i+1}, h_{i+1}). \tag{24}$$

According to the application at hand, we can fix the outermost one to three rows ($k = 0, 1, 2$) to retain C^0, G^1 or G^2 interpolation properties. Then the equation system can be solved in a least-squares sense. The initial parameterization can be generated by projecting the data points on an initial surface. If the deviation of the fitted surface is above tolerance, we can elevate the patch degree, re-parameterize the points, and fit again.

5.4.1. Smoothing

The above approximation method is optimal in a sense, but the computed control points may wiggle and thus be inappropriate for further design. It is standard practice to add some kind of smoothing term T to the system, that may slightly decrease accuracy, but yields better control point positions. The expression to be minimized is thus adjusted to

$$\sum_i (S(u_i, v_i) - P_i)^2 + \sigma T = \min, \tag{25}$$

where σ is a smoothness parameter controlling the extent of fairing.

A simple technique for reducing the oscillation of control points is to pull each point towards the center of mass of its neighbors. In the case of GB patches, this is done by setting

$$T = \sum_{i=1}^{n} \sum_{j=1}^{\lfloor d/2 \rfloor} \sum_{k=1}^{l-1} T^i_{j,k} + T_{l,l}, \tag{26}$$

where

$$T^i_{j,k} = \left(C^{d,i}_{j,k} - \frac{1}{4}\left(C^{d,i}_{j-1,k} + C^{d,i}_{j+1,k} + C^{d,i}_{j,k+1} + C^{d,i}_{j,k-1} \right) \right)^2, \qquad T_{l,l} = \begin{cases} \left(C^d_{l,l} - \frac{1}{n} \sum_{i=1}^n C^{d,i}_{l-1,l-1} \right)^2 & \text{when } d \text{ is even,} \\ 0 & \text{when } d \text{ is odd.} \end{cases} \tag{27}$$

Here indexing is naturally extended to include control points $C^{d,i}_{j,l}$, with $C^{d,i}_{l,l} = C^d_{l,l}$ for even degrees.

6. Case studies

In this section a few examples are given to demonstrate some applications of GB patches.

6.1. Fitting examples

We have discussed in Section 5.1 that degree elevation is not exact for GB patches. Its precision can be enhanced by the above fitting algorithm. Table 1 lists the results of elevating a 5-sided quintic patch to degrees 6–10 with and without fitting. Some of the surfaces are shown in Figure 9. While degree elevation produced a maximum deviation of roughly 0.2% of the bounding box diagonal, fitting reduced this to 0.01%. The average error has been improved from roughly 0.05% to less than 0.005%.

d	maximum	average	maximum after fit	average after fit
6	0.175%	0.056%	0.010%	0.003%
7	0.129%	0.038%	0.016%	0.004%
8	0.217%	0.067%	0.015%	0.003%
9	0.218%	0.064%	0.012%	0.003%
10	0.273%	0.082%	0.013%	0.003%

Table 1: Improving degree elevation of a quintic patch by fitting. Values are given as percentages of the diagonal of the bounding box. The underlying mesh contains approx. 2500 triangles, with an average edge length of $\approx 1\%$.

As another example, Figure 10 shows a general topology curve network drawn over the triangular mesh model of a concept car with 67802 triangles and a bounding box diagonal of approximately 6700 millimeters. A patch complex of one four sided and two five-sided surfaces of degree 7 is shown. The fitted surfaces have a maximum deviation of $\approx$ 15mm, while the average deviation is $\approx$ 3mm. These correspond to $\approx 0.22\%$ and $\approx 0.04\%$ with respect to the bounding box diagonal.

6.2. Curvenet-based models

The next two examples are based on free-form models that were also used for testing in Pan et al. [7]. The input is given in the form of very dense polylines. For our application these are converted into a free-form network of parametric curves. In addition to the boundaries, G^1 cross-derivatives in Bézier form are computed (see for example Wang et al. [12]); these are sufficient to ensure smooth connections between the adjacent GB patches and create a full patchwork.

The first test model is a torso that interpolates a network of 40 curves (Figure 11). The model contains altogether 40 patches: 8 three-sided, 28 four-sided and 4 seven-sided. These last ones under the shoulder represent the main challenge from a modeling point of view, as they have to interpolate seven boundaries located in a very peculiar manner in 3D. This example is good to demonstrate how merging of different degree interpolants work. As it can be seen in Figures 11c–11d, there are three cubic, two quintic and two sextic boundaries, representing simple and more complex curves. The final patch is a united structure of a degree 6 patch, reproducing each interpolant. The cubic and quintic boundaries and cross-derivatives have been degree elevated, and appropriate interior control points were inserted during the elevation process.

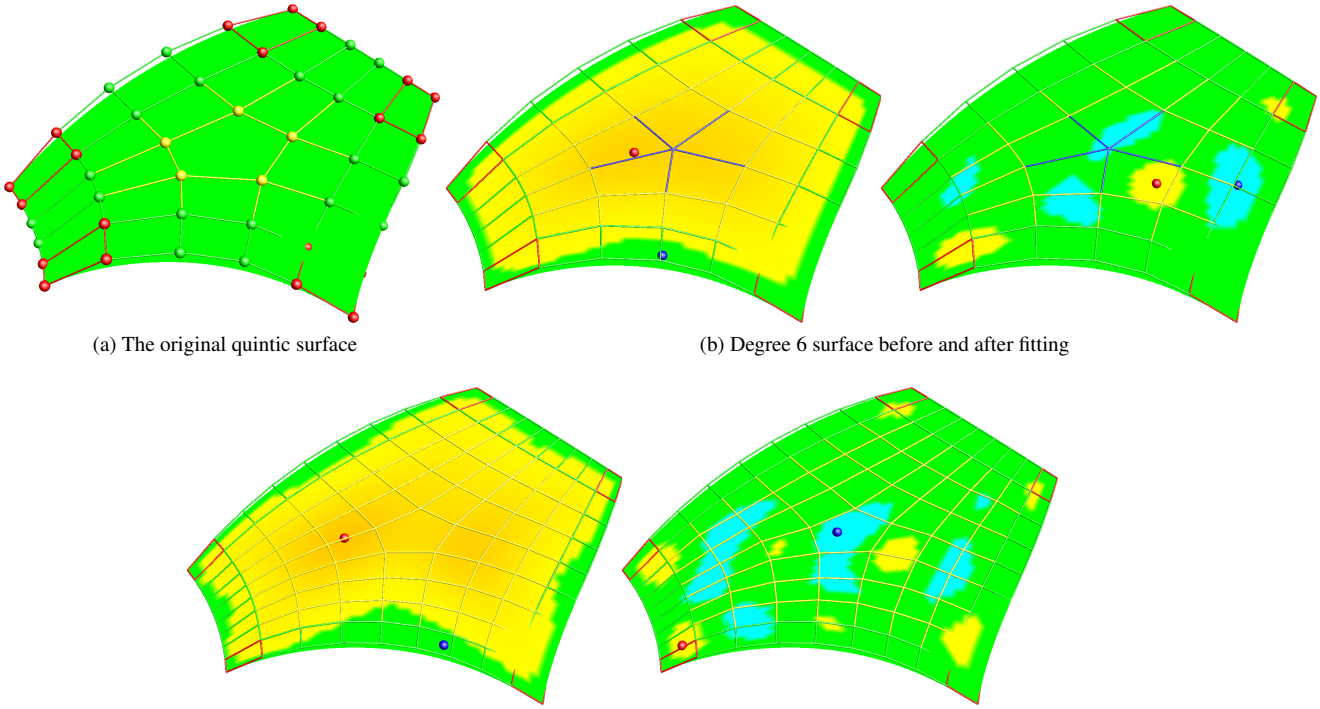

(a) The original quintic surface

(b) Degree 6 surface before and after fitting

(c) Degree 9 surface before and after fitting

Figure 9: Degree elevation of a quintic surface with deviation map (red $>$ 0.5%, 0.005% $>$ green $>$ -0.005%, -0.5% $>$ blue). Red and blue markers show the position of the maximal positive and negative deviations, respectively.

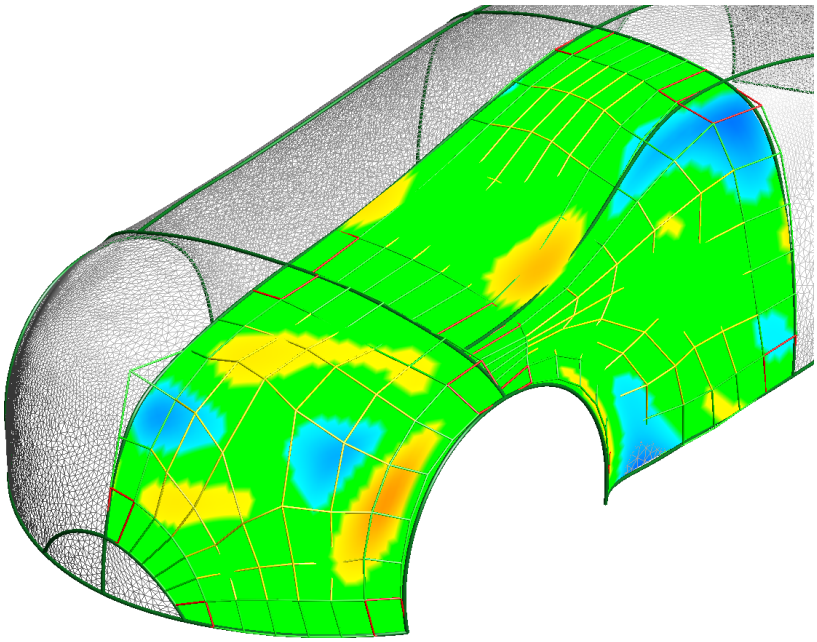

Figure 10: Fitted surfaces on a concept car mesh with deviations (red $>$ 20mm, 5mm $>$ green $>$ -5mm, -20mm $>$ blue).

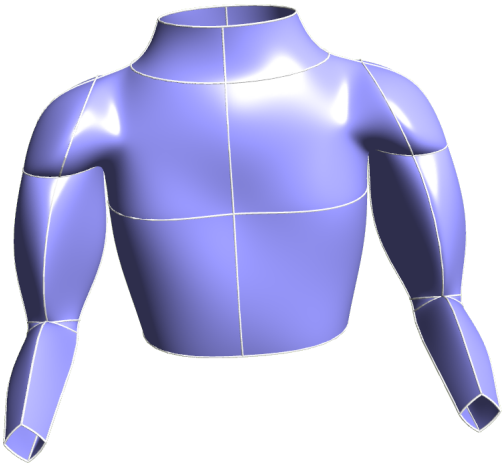

(a) The whole shaded model

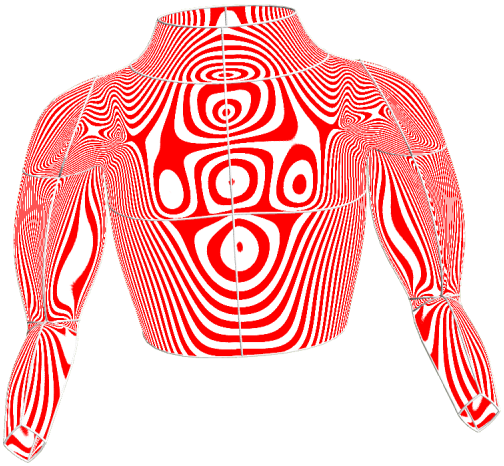

(b) Isophote lines

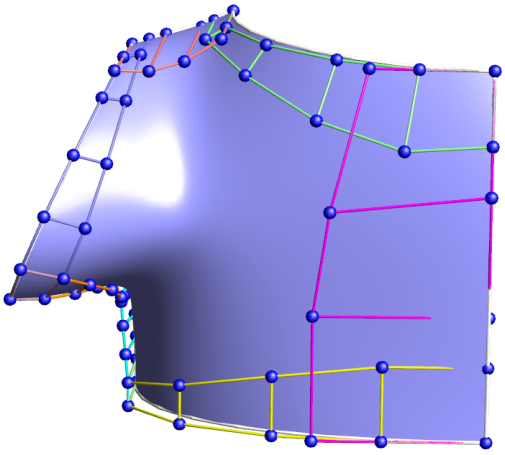

(c) A 7-sided patch with side interpolants of various degrees

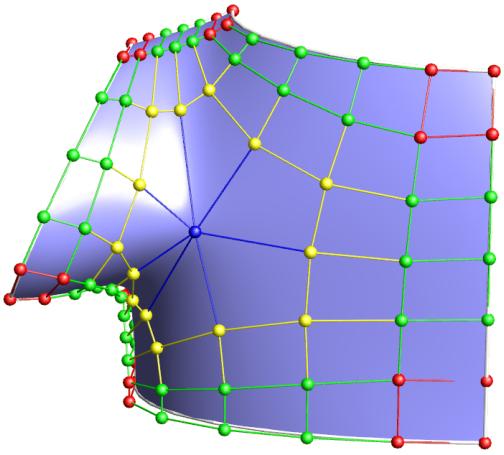

(d) Side interpolants unified to a common degree

Figure 11: "Torso" model .

The gamepad model (Figure 12) is defined by 10 curves (2 open, 8 closed). The model contains 44 patches, fitted fully automatically to the given network. There are 18 three-sided, 18 four-sided, 6 five-sided and 2 six-sided patches. Figures 12a–12c show the defining ribbon structure that ensures G^1 continuity; contouring and a mean curvature map illustrate smoothness, while in Figure 12d the control structures of a five-sided and a six-sided patch are shown.

Conclusion

We have investigated a multi-sided Bézier surface representation with a simple control structure. GB patches are generalizations of quadrilateral Bézier patches, preserving many of their favorable properties. In this representation control points are associated with a combination of blending functions depending on side-based parameters; these satisfy boundary constraints in the same way as for quadrilateral patches.

This paper focused on various issues to enhance the former GB representation. The new control structure is a better match for the quadrilateral structure; modified blending functions ensure higher-degree continuity, and a better control is gained over the interior. It has also been shown that the most important algorithms of quadrilateral patches can be adapted for GB patches, including shape control, degree elevation and reduction, and mesh approximation by n-sided patches.

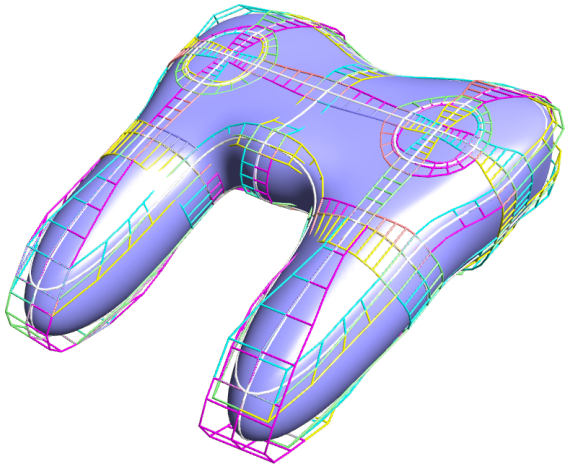

(a) Side interpolant control nets

(b) Contours showing G^1 continuity

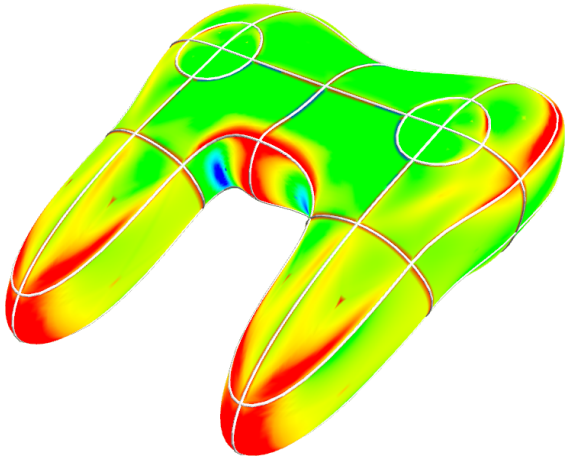

(c) Mean curvature

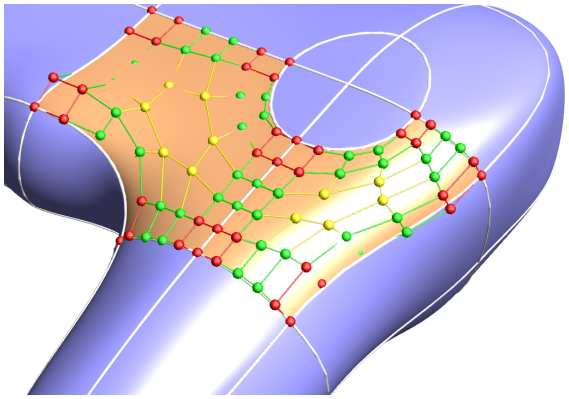

(d) Control net of two patches

Figure 12: "Gamepad" model

There are interesting problems for future work. It would be nice to replace the rational weighting terms by another, suitable parameterization. Using concave domains for GB patches is also challenging. Finally, a similar approach to create a multi-sided B-spline patch is a topic of interest, as well.

Acknowledgements

All images were generated by the Sketches prototype system (ShapEx Ltd, Budapest); the authors appreciate the exceptional programming contribution of György Karikó. The third author has been supported by the UNKP-16-3-I. New National Excellence Program of the Hungarian Ministry of Human Resources. The test suit of free-form objects defined by curve networks has been made public by Pan et al. [7]; we have found this very useful for our work and also for the CAGD research community.

Appendix A. Correction terms for the new parameterization

In Eq. (11) in Section 4.1, we have defined a modified parameterization with two correction terms, W_i^1 and W_i^2. For $n = 5, 6$ we define W_i^1 as $c_n \lambda_{i-2} \lambda_{i+1}$; for $n = 7, 8$ as $2\lambda_{i-2}\lambda_{i+1} + c_n(\lambda_{i-2}\lambda_{i+2} + \lambda_{i+1}\lambda_{i-3})$. Here c_n denotes a constant:

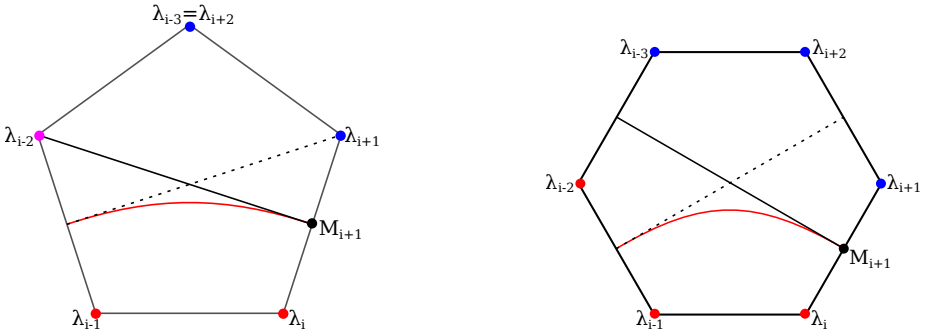

(a) $n = 5$ (b) $n = 6$

Figure A.13: The constant parameter line $h_i = \frac{1}{2}$ is perpendicular to sides $i - 1$ and $i + 1$.

$c_n = 1$ for odd, and $c_n = 2$ for even number of sides. As n grows, at every second n, two new terms will be added to the expression. The general formula (valid for $n \geq 7$) is

$$W_i^1(\lambda_1, \ldots, \lambda_n) = 2\lambda_{i-2}\lambda_{i+1} + \lambda_{i-2}\left(\sum_{j=i+2}^{i+m+1} 2\lambda_j + c_n\lambda_{i+m+2}\right) + \lambda_{i+1}\left(\sum_{j=i-m-2}^{i-3} 2\lambda_j + c_n\lambda_{i-m-3}\right), \tag{A.1}$$

where $m = \lfloor (n-7)/2 \rfloor$.

Here we prove the tangential property only for $n = 5, 6$ (see Figure A.13); generalization for higher values of n is straightforward. Due to symmetry, it is sufficient to show that the $h_i = \frac{1}{2}$ constant parameter line is perpendicular to side $i + 1$ at point M_{i+1}. In other words, we need to prove that the derivative of h_i,

$$h_i' = -\lambda_{i-1}' - \lambda_i' - c_n(\lambda_{i-2}'\lambda_{i+1} + \lambda_{i-2}\lambda_{i+1}') \tag{A.2}$$

is zero along the perpendicular direction. (We can disregard the W_i^2 term here, as it does not effect this property at the endpoints, see below.) At point M_{i+1} we have $\lambda_{i-2} = 0$ and $\lambda_{i+1} = \frac{1}{2}$, thus $h_i' = -(\lambda_{i-1}' + \lambda_i' + \frac{1}{2}c_n\lambda_{i-2}')$. Symmetrically, based on side $i + 2$, this can also be written as $h_i' = -(\lambda_{i+2}' + \lambda_{i+1}' + \frac{1}{2}c_n\lambda_{i+3}')$. We can see that adding these two expressions results in $2h_i' = \sum_{i=1}^n \lambda_i'$ (in the five-sided case this is because $\lambda_{i-2} = \lambda_{i+3}$). But we also have $\sum_{i=1}^n \lambda_i$=1, consequently $2h_i' = \sum_{i=1}^n \lambda_i' = 0$.

We continue with the W_i^2 term. For $n = 5$ define W_i^2 as $\delta_n\lambda_{i-2}\lambda_{i+1}\lambda_{i+2}$, for $n = 6$ as $\delta_n\lambda_{i-2}\lambda_{i+1}(\lambda_{i-3} + \lambda_{i+2})$. In general, the expression can be written as

$$W_i^2(\lambda_1, \ldots, \lambda_n) = \delta_n\lambda_{i-2}\lambda_{i+1}\left(1 - \sum_{j=i-2}^{i+1} \lambda_j\right), \tag{A.3}$$

i.e., in the parentheses we sum up only the distant vertices excluding those that belong to sides $i - 1$, i and $i + 1$. It is easy to see that W_i^2 has no effect on any side of the polygon, it just adjusts the fullness of the arcs, and by means of δ_n we can force h_i to go through any prescribed point.

The circular constraint computation is simple, using trigonometric equations. We determine the center point O of the imaginary circle as the intersection of sides $i - 1$ and $i + 1$, and compute its radius as the distance between O and the related midpoint M_{i+1} on the polygon. From this we can determine the barycentric coordinates of the center of the arc, and substitute into Equation (A.3) in order to express δ_n. These values depend on n, see Table A.2.

	$n = 5$	$n = 6$	$n = 7$	$n = 8$	$n = 9$	$n = 10$
δ_n	3.61787	5.36603	8.05399	9.89736	10.08788	10.08235

Table A.2: Values of δ_n for different number of sides.

Note: for $n = 3$ a similar circular arc parametrization with three constrained points can be applied. Having $1 - \lambda_{i-1} - \lambda_i = \lambda_{i+1}$ and using only a single W_i^2 term, we obtain

$$h_i(u, v) = \lambda_{i+1} + \delta_3 \lambda_{i-1} \lambda_i \lambda_{i+1},$$

and $\delta_3 \approx 2.19615$ can be calculated as before.

References

[1] Ball, A. A., Zheng, J., 2001. Degree elevation for n-sided surfaces. Computer Aided Geometric Design 18 (2), 135–147.
[2] Floater, M. S., 2015. Generalized barycentric coordinates and applications. Acta Numerica 24, 161–214.
[3] Hosaka, M., Kimura, F., 1984. Non-four-sided patch expressions with control points. Computer Aided Geometric Design 1 (1), 75–86.
[4] Kahmann, J., 1983. Continuity of curvature between adjacent Bézier patches. In: Surfaces in computer aided geometric design. North Holland, pp. 65–75.
[5] Krasauskas, R., 2002. Toric surface patches. Advances in Computational Mathematics 17 (1), 89–113.
[6] Loop, C. T., DeRose, T. D., 1989. A multisided generalization of Bézier surfaces. ACM Transactions on Graphics 8 (3), 204–234.
[7] Pan, H., Liu, Y., Sheffer, A., Vining, N., Li, C.-J., Wang, W., 2015. Flow aligned surfacing of curve networks. ACM Transactions on Graphics 34 (4), 127.
[8] Sabin, M., 1983. Non-rectangular surface patches suitable for inclusion in a B-spline surface. In: EuroGraphics. North Holland, pp. 57–70.
[9] Sabin, M., 1986. Some negative results in n-sided patches. Computer-Aided Design 18 (1), 38–44.
[10] Sun, L.-Y., Zhu, C.-G., 2015. G^1 continuity between toric surface patches. Computer Aided Geometric Design 35, 255–267.
[11] Várady, T., Salvi, P., Karikó, G., 2016. A multi-sided Bézier patch with a simple control structure. Computer Graphics Forum 35 (2), 307–317.
[12] Wang, W., Jüttler, B., Zheng, D., Liu, Y., 2008. Computation of rotation minimizing frames. ACM Transactions on Graphics 27 (1), 2.
[13] Warren, J., 1992. Creating multisided rational Bézier surfaces using base points. ACM Transactions on Graphics 11 (2), 127–139.
[14] Zheng, J., Ball, A. A., 1997. Control point surfaces over non-four-sided areas. Computer Aided Geometric Design 14 (9), 807–821.